The Journal of Supercritical Fluids 228 (2026) 106778

Contents lists available at ScienceDirect

The Journal of Supercritical Fluids

journal homepage: www.elsevier.com/locate/supflu

Exploring cluster formation in CO_2 + hydrocarbon mixtures: From binary to ternary systems

Ariel A. Acuña [a,b], Manuela Artal [b], Guillaume Galliero [a], Jean-Luc Daridon [a,*]

[a] Laboratoire des Fluides Complexes et leurs Réservoirs, Univ. of Pau and Pays de l'Adour/CNRS, E2S, UMR 5150, Pau 64000, France
[b] Departamento de Química Física, Facultad de Ciencias, Universidad de Zaragoza, Zaragoza, Spain; Instituto agroalimentario de Aragón – IA2 (Universidad de Zaragoza – CITA), Zaragoza, Spain

HIGHLIGHTS

- New density data in CO_2 + n-C_7, CO_2 + n-C_{12} binary systems.
- Density data in CO_2 + n-C_7 + n-C_{12} ternary system.
- Derivations of partial molar volume at infinite dilution.
- Determination of clustering effect in binary and ternary systems.
- Combining rule for clustering effect with multi solutes in CO_2.

GRAPHICAL ABSTRACT

Cluster size of binary and ternary systems, where ●; (binary CO_2-C_7 and CO_2-C_{12} systems), × ; (ternary CO_2-C_7-C_{12} system) and –; (linear correlation).

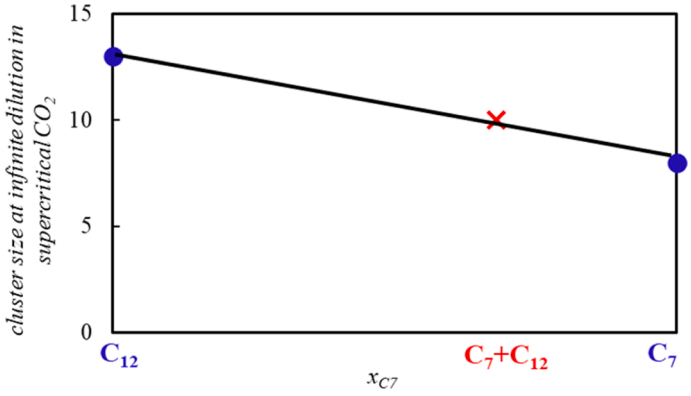

ARTICLE INFO

Keywords:
CO_2
Hydrocarbons
Mixtures
Supercritical Fluid
Clusters
SAFT

ABSTRACT

This study aims to investigate clustering phenomena at infinite dilution in supercritical CO_2-rich mixtures with n-heptane (*n*-C_7) and n-dodecane (*n*-C_{12}), in both binary and ternary systems. The main objective is to understand how the individual clustering behaviors of the solutes combine in the ternary mixture, and whether this combination follows an additive rule. To this end, density measurements were carried out at 313.15 K and 323.15 K over a pressure range of (10–70) MPa, enabling the determination of partial molar volumes as indicators of clustering. The results reveal a pronounced clustering effect at low pressures (below 20 MPa) for both binary and ternary systems, as evidenced by strongly negative partial molar volumes, which indicate the formation of compact solvation clusters around the solutes. In the ternary mixture, the clustering behavior was found to follow a nearly linear combination, based on the mole fractions of the clusters observed in the binary systems. This suggests that clustering in CO_2 + multi-solute systems may be predicted from binary behavior.

Two SAFT-type equations of state (PC-SAFT and SAFT-VR Mie) were employed to evaluate their ability to model the transition from binary to ternary systems. While both captured the non-ideal volumetric behavior,

* Corresponding author.
E-mail addresses: aaacuna@univ-pau.fr (A.A. Acuña), martal@unizar.es (M. Artal), guillaume.galliero@univ-pau.fr (G. Galliero), jean-luc.daridon@univ-pau.fr (J.-L. Daridon).

https://doi.org/10.1016/j.supflu.2025.106778
Received 6 June 2025; Received in revised form 3 September 2025; Accepted 4 September 2025
Available online 6 September 2025

SAFT-VR Mie demonstrated better quantitative agreement. These findings improve our understanding of solute–solvent interactions in CO_2-rich environments and support enhanced modeling of processes such as supercritical extraction, carbon capture and storage (CCUS), and enhanced oil recovery (EOR).

1. Introduction

The knowledge of the thermophysical properties of carbon dioxide+hydrocarbon mixtures at supercritical states has become increasingly important in recent years for their importance for developing more efficient process design, such as supercritical fluid extraction (SFE), carbon capture, utilisation and storage (CCUS), enhanced oil recovery (EOR), synthesis of valuable chemicals and, more recently, research into the use of CO_2 for recycling as part of circular economy [1–5]. In particular, throughout the decades, supercritical CO_2 has emerged as a prominent solvent due to its characteristics, which allows for efficient extraction and separation process. Its critical temperature close to room temperature ($T_c = 304.23$ K) and critical pressure lower than 10 MPa ($p_c = 7.38$ MPa) makes it an attractive alternative to more harmful solvents used in industry.

However, volumetric properties of CO_2-solute systems in the supercritical state are not widely documented in the literature. To address this gap, our group initiated a series of experimental studies [6–9] on the thermophysical characterization of asymmetric CO_2 + *n*-alkane binary mixtures. In the present work, we extend the data reported in previous articles for two binary mixtures: CO_2 + *n*-C_7 and CO_2 + *n*-C_{12}, broadening the experimental range up to infinite dilution of hydrocarbon. Furthermore, we enlarge the data set by investigating a ternary system formed by the addition of carbon dioxide in a mixture of *n*-heptane + *n*-dodecane at a fixed composition. For both binary and ternary mixtures, density measurements were taken along two supercritical isotherms slightly above the critical temperature of CO_2 (313.15 K and 323.15 K) at pressures ranging from (10−70) MPa, focusing on the composition range from (90–99.8) mol% of CO_2. In addition, two Equation of State (EoS) of the Statistical Associating Fluid Theory (SAFT) type [10,11] were used and their results compared with experimental data. These equation were selected based on their solid theoretical foundations.

The extension of the previously published data to higher concentration of CO_2 was motivated by the observation that CO_2 + hydrocarbon systems may, rather surprisingly, exhibit non-ideal behaviour at hydrocarbon near-infinite dilution above the CO_2 critical point. In this region, the system shows strong density variation with the solute amount. This behaviour is attributed to clustering phenomenon [12], which leads to variations in thermophysical properties, potentially impacting the efficiency of applications involving CO_2 as a supercritical solvent. Clusters are defined as agglomerates of solvent molecules around a solute molecule, resulting in a shrinkage of the system, evidenced by a decrease of the partial molar volume of the solute which can reach negative values in some systems [6]. This behavior can be characterized by determining the cluster size from partial molar volumes and isothermal compressibility of CO_2 [12], which has been confirmed by molecular dynamics simulations [13]. Consequently, our research focuses on the analysis of near-infinite dilution systems with supercritical CO_2 as solvent, which remain insufficiently explored in the existing literature. Specifically, our objective is to study the clustering phenomenon and to evaluate the impact of the solute using both one species and a binary mixture. This approach allows us to determine whether the clustering phenomenon exhibits additivity in such systems. Additionally, this study aims to assess the precision and reliability of specific equations of state (EoS) in reproducing the experimental data presented in this work, both qualitatively and quantitatively.

The work is structured as follows: Section 2 details the materials and methods used, including the use of a modified U-shaped density meter that allows liquid injection by syringe, along with the methodology to determine the uncertainties of the densities and partial molar volumes. Section 3 provides a brief theoretical background of the SAFT equations of state used in this work. Section 4 presents the results and discussion for the three systems investigated. The results of partial molar volumes at infinite dilution derived from density data are presented and discussed in Section 5, as well as the cluster size determination and the connection between the binary and ternary mixtures near the CO_2 critical point. Finally, the main results of the present work are summarized in Section 6.

2. Materials and methods

2.1. Materials

Carbon dioxide was purchased from LINDE with a nominal purity of 99.995 % while *n*-heptane and *n*-dodecane were obtained from ThermoFisher Scientific with a purity of 99.5 % and from Sigma-Aldrich with a purity of 99.6 %, respectively. Given the high purity of the hydrocarbons (above 99.5 %) and the range of highly CO_2-rich mixtures ($x_{CO_2} > 90$ % mol), the contribution of hydrocarbon impurities is negligible compared to other uncertainties. In other words, considering the worst-case configuration and assuming a 10 % fractional density difference between the sample of interest and the impurity, the contribution to the uncertainty of the impurities claimed by the manufacturer is approximately 0.003 %[14]. Moreover, the impact of these impurities on CO_2 is even smaller. The sources and purities of pure components used for the preparation of the investigated mixtures are summarized in Table 1. All compounds and their mixtures were used without any further treatment.

2.2. Apparatus

The experimental apparatus used for measuring the density, ρ, in gas + liquid mixtures was described in detail in a previous article [6]. An Anton Paar vibrating U-tube densimeter was utilized for measuring densities according to the experimental setup shown in Fig. 1. A set of high pressure volumetric pumps was used for working with gas+liquid mixtures under pressure. The first pump was used for preparation and homogenization of mixtures. It was connected to a CO_2 tank placed on a high mass high precision balance with an standard uncertainty of 0.001 g, enabling the weighing of the injected CO_2. The CO_2 tank is connected to the flow cell via a flexible PEEK tube (1/16") to avoid disturbances to the balance during gas weighing. The gas mass is therefore determined by tank weight during filling. The second pump controlled and maintained the pressure above the bubble point during the transfer from the first pump to the chamber of the densimeter. An external Huber thermostatic bath, with a stability of 0.05 K, regulates the temperature of the densimeter while a temperature sensor (Pt 100) is positioned inside the jacket to monitor temperature with an standard uncertainty of 0.05 K. The pressure is measured throughout the complete range with a Presens manometer with an standard uncertainty of 0.02 %. To achieve the desired solute near-infinite dilution composition, a specific technique has been developed in this work. For this purpose, the configuration previously used for mixture preparation [6] was

Table 1
Purity of Chemicals.

Chemical	CAS	Manufacturer	Purity
carbon dioxide	124–38–9	France	99.995 %
n-heptane	142–82–5	Germany	≥ 99.5 %
n-dodecane	112–40–3	Germany	≥ 99.6 %

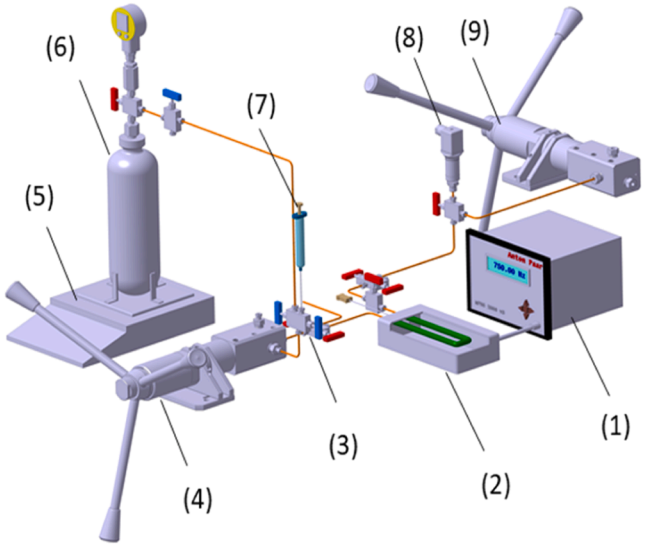

Fig. 1. Schematic view of the density measurement setup. **(1)** Anton Paar, **(2)** U-shape tube, **(3)** 3-Way/2-Stem High Pressure Needle Valve, **(4)** Pump n°1 for homogenization and transfer, **(5)** Precision balance, **(6)** Gas Tank, **(7)** Liquide injection syringe, **(8)** Pressure Gauge, **(9)** Pump n°2 for isobar transfer.

modified. The standard uncertainties in mass introduced were estimated to be 0.001 g for hydrocarbons where the resulting combined expanded uncertainty in the mole % of CO_2 calculated with the coverage factor ($k = 2$) to obtain the expanded uncertainties $U(x_{CO_2})$ (level of confidence = 0.95) are presented in Table 2.

As shown in Fig. 2, a 3-way/2-stem High Pressure Needle Valve was added in the setup for precise injection of gas and liquid. This modification makes the injection system versatile, allowing for preparing gas + liquid mixtures in various composition ranges from (90–99.8) mol% of CO_2. It should be pointed out that one inlet port is ended by a rubber septum to prevent solute reflux during addition of liquid using a syringe.

Before preparing the mixture, vacuum is achieved in the pump. The liquid is then added using a syringe, with the needle positioned in contact with the valve's stem after piercing the septum. When the valve is opened, the liquid in the syringe is drawn into the cell by vacuum suction. The amount of liquid injected is accurately determined by performing a double weighing of the syringe. For systems involving two hydrocarbons, the liquid mixture is prepared on a precision balance off-site of the densimeter by mass weighing and then placed into the injection syringe. Following this operation, CO_2 is injected at constant pressure (5.5 MPa at room temperature) from its storage tank, with the mass monitored during the injection. After injection of both liquid and gas components, the system is pressurized to a final pressure of 70 MPa.

Table 2
Combined expanded uncertainty $U(xCO_2)$ in mol% of CO_2 for all the system investigated.

$CO_2 + n$-C_7		$CO_2 + n$-C_{12}		$CO_2 + n$-$C_7 + n$-C_{12}	
x_{CO_2} mol%	$U(x_{CO_2})^a$	x_{CO_2} mol%	$U(x_{CO_2})^a$	x_{CO_2} mol%	$U(x_{CO_2})^a$
89.39	0.006	90.00	0.004	90.00	0.005
93.00	0.006	94.02	0.004	93.03	0.007
96.00	0.008	96.00	0.004	96.00	0.006
98.00	0.006	98.20	0.004	98.03	0.006
99.28	0.006	99.20	0.004	99.30	0.004
99.79	0.005	99.50	0.004	99.80	0.004

$^aU_c(x_{CO_2}) = k * \left(x_{CO_2}(1 - x_{CO_2}) \left[\frac{u^2(m_{CO_2})}{m^2_{CO_2}} + \frac{u^2(m_{C_x})}{m^2_{C_x}} \right]^{0.5} \right)$

m_{C_x}; mass of alkanesm_{CO_2}; mass of CO_2

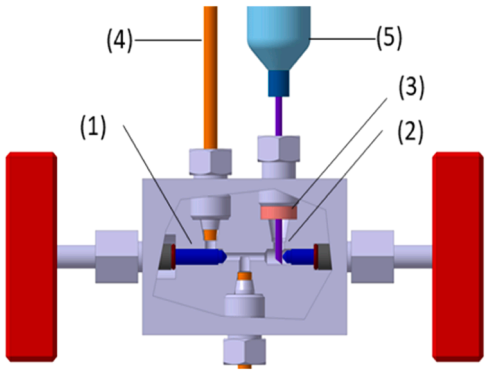

Fig. 2. Enlarged view of the 3-Way/2-Stem High Pressure Needle Valve, **(1)** CO_2 injection valve, **(2)** Liquid injection valve, **(3)** rubber septum, **(4)** CO_2 injection tubing and **(5)** Liquid injection syringe.

This pressure is significantly above the bubble point pressures of the investigated systems, which were measured to be below 12 MPa for CO_2–n-C_7 [15–18], and even lower for the CO_2–n-C_{12} [19] system, regardless of composition and for both isotherms considered. For the ternary mixture, no experimental phase equilibrium data could be found. However, a preliminary estimation using the PPR78 model [20], which is particularly well suited for predicting phase equilibria in such CO_2 + alkane systems [21,22], indicates that the bubble point pressures also remain below 12 MPa within the temperature range investigated.

The second pump remains closed during the homogenization and stabilization of temperature. After several cycles of homogenization thanks to the reciprocating motion of the tungsten ball in the pump, the sample is transferred at high pressure to the U-tube densimeter by moving the pistons of the 2 pumps in opposite directions. This high-pressure transfer is essential to avoid any drop in pressure below the bubble point during the transfer, thereby maintaining the homogeneity of the system throughout the complete transfer process. To avoid a sudden drop in pressure when opening the pump containing the initially prepared mixture, the U-tube densimeter is fully charged with a buffer of the same components at high pressure. This buffer solution is displaced by the solution in the first pump. Finally, after displacing more than three times the volume of the densimeter, the transfer is considered as complete, and the outlet valve is closed.

By measuring the period τ of vibration of the tube containing the sample, the density ρ is determined according to the following linear relation in terms of the square of the resonance period τ^2:

$$\rho(T,p) = A(T,p) \quad \tau^2 - B(T,p) \tag{1}$$

where the coefficients A and B are related to temperature and pressure according to the robust physically-based model proposed by May et al. [23,24] for representing the vibration behavior of a U-tube densimeter:

$$A(T,p) = \frac{A_0(1+\beta_\tau p)}{\left(\left(1+\varepsilon_1(T-T_0)+\varepsilon_2(T-T_0)^2\right)^2(1+\alpha_v(T-T_0)+\beta_v p)\right)} \tag{2}$$

$$B(T,p) = \frac{B_0}{(1+\alpha_v(T-T_0)+\beta_v p)} \tag{3}$$

The seven apparatus parameters (A_0, B_0, α_v, β_v, β_τ, ε_1, ε_2) were obtained through calibration with water and nitrogen, as well as measurements of the U-tube cell under vacuum. The measured vacuum periods allow for the determination of the ratio B_0/A_0 and the parameters ε_1 and ε_2. Calibration with nitrogen, using values provided by [25], was necessary for measuring in the low-density domain (here for pressure below 20 MPa), whereas calibration with water density values [26] was required for high-density measurements.

The combined standard uncertainty $u_c(\tau)$ in resonance period measurements for τ, τ_{vacuum} , τ_{H2O} and τ_{N_2} was determined by the quadratic sum of different source of uncertainty in measurement of resonance period $u(\tau)$ as well as temperature $u(T)$ and pressure $u(p)$, each weighted by the respective partial derivatives of τ with respect to these variables as proposed by Guidelines for evaluating and expressing the uncertainty of NIST measurement results [28]:

$$u_c^2(\tau) = [u(\tau)]^2 + \left(\frac{\partial \tau}{\partial T}\right)_p [u(T)]^2 + \left(\frac{\partial \tau}{\partial p}\right)_T [u(P)]^2 \quad (4)$$

A statistical-based calculation method has been implemented to propagate $u_c(\tau)$, $u_c(\tau_{\text{vacuum}})$, $u_c(\tau_{H_2O})$ and $u_c(\tau_{N_2})$, as well as the uncertainties in the densities of the calibration fluids $u(\rho_{H_2O})$, $u(\rho_{N_2})$ in the determination of the standard uncertainty in density $u(\rho)$. In this method [27] a random normal distribution perturbation of 5000 points is generated around each experimental period and, from these perturbed periods, a distribution of densities were calculated using Eqs. 2 and 3. The standard deviation of the obtained distribution is taken as the standard uncertainty in the density measurement which is then multiplied by the coverage factor ($k = 2$) to obtain the expanded uncertainties $U(\rho)$ (level of confidence = 0.95). Each set of perturbed density data are then used to derive the partial molar volume PMV according to the method proposed in a previous article [27].

3. Modelling

Two SAFT equations of state (EoS): PC-SAFT [28] and SAFT-VR Mie [11] were tested to investigate their potential for predicting the partial molar of hydrocarbon solutes at near-infinite dilution in supercritical carbon dioxide. Both equations of state contains different terms in the reduced Helmholtz energy, including contributions from an ideal gas, hard-chain (for PC-SAFT), monomer (for SAFT-VR Mie), dispersion, as well as association. However, in our current study, the association contribution was not used due to the lack of association among components in the investigated mixtures.

This type of molecular based EoS, initially proposed by Chapman et al. [10] by applying Wertheim's theory of associating fluids [29] to chain molecules, is now extensively used in the fields of materials science and chemical engineering due to its accurate prediction of thermodynamic properties of both liquids and gases mixtures. Although these EoS are based on theoretical foundations, they require adjustments of their parameters to provide quantitative results for pure component properties. For mixtures, mixing rules are needed. In them, it is usual to include a non-zero binary interaction parameter (k_{ij}) if they are asymmetric as those studied in this work.

The PC-SAFT EoS was developed by Gross and Sadowski [28], by considering a hard-chain reference constituted of spherical segments connected in pairs by the modified square-well potential proposed by Chen and Kreglewski [30]. They introduced a Barker-Henderson-type perturbation to capture the attractive interactions between these chains. Accordingly, for a non-associating molecule, the residual molar Helmholtz energy a^{res} is written as the sum of two contributions, as follows:

$$a^{\text{res}} = a^{\text{hc}} + a^{\text{disp}} \quad (5)$$

The first term is the contribution from the hard chain reference fluid, the second represents the perturbation contribution, which take into account attractive interactions. A comprehensive development of these terms is provided in [28]. The equation requires three parameters to describe the non-associated fluids: the number segment m_s, the diameter of spherical segment σ, and the energy parameter ε/k. In this work, PC-SAFT was implemented using VLXE advanced *pVT* simplified software [31].

Lafitte et al. [11] developed a statistical associating fluid theory for variable range interactions (SAFT-VR) of the Mie form (SAFT-VR Mie), which is implemented in the Templated Equation of State Package software (teqp) developed by Bell et al. [32]. This implementation employs advanced numerical techniques without relying on analytical derivatives, facilitating EoS implementation without a loss of precision. In this EoS, the molecules are considered as a chain formed from spherical monomers with repulsive and attractive interactions through the Mie potential $u^{\text{Mie}}(r)$, which is defined as:

$$u^{\text{Mie}}(r) = \frac{\lambda_r}{\lambda_r - \lambda_a}\left(\frac{\lambda_r}{\lambda_a}\right)^{\frac{\lambda_r}{\lambda_r-\lambda_a}} \varepsilon\left(\left(\frac{\sigma}{r}\right)^{\lambda_r} - \left(\frac{\sigma}{r}\right)^{\lambda_a}\right) \quad (6)$$

where r is the distance between the segments, λ_r and λ_a are the repulsive and attractive exponents, ε is the potential depth and σ is the diameter of monomers. In the absence of association between molecules, the residual molar Helmholtz energy is also written as the sum of different contributions:

$$a^{\text{res}} = m_s a^{\text{Mono}} + a^{\text{disp}} + a^{\text{chain}} \quad (7)$$

where m_s is the number of segments, and a^{Mono} is the Helmholtz energy of Mie monomers. It is obtained from the Mie potential using Barker-Henderson [33] perturbation expansion. The third term represents the contribution due to chain formation of Mie segments. It was obtained from Wertheim's first-order perturbation theory (TPT1) function. A detailed description and development of these terms is set out in detail in [11]. In addition to the three parameters (m_s, σ, ε/k), parameters must be added to account for Mie potential characteristics: one for the repulsive term λ_r and and one attractive λ_a interaction [11,34].

The parameters for pure components used in this work were sourced directly from the literature and taken from the original publications on the development of PC-SAFT [28] and SAFT-VR Mie [11], as listed in Table 3. Also, the binary interaction parameters (BIPs) were determined by fitting densities predicted by the EoS with those obtained from experiments. The goal is to minimize the difference between the calculated and experimental density values. This method relies on an iterative process. In particular, the approach implemented in the Templated Equation of State Package (teqp) software requires an initial guess for the co-existing densities and compositions. For a more detailed explanation of the model, see Ref. [32]. PC-SAFT and SAFT-VR Mie are both based on the same SAFT framework but differ by their treatment of the dispersion forces. In PC-SAFT, the Barker-Henderson perturbation is added to the hard chain to account for the attraction between chains whereas it is considered at the monomer level in SAFT-VR Mie. Moreover, the variable range in SAFT-VR Mie, allows flexibility in adjusting the repulsive interaction and attractive range, making it applicable across variable range of interactions, from soft to highly repulsive, and for short-range Mie potentials. A key feature of this approach is its significantly enhanced accuracy in the near-critical region [34].

4. Results and discussion

4.1. Pure compounds

The densities of pure CO_2, *n*-C_7, and *n*-C_{12} were measured at temperatures of 313.15 K and 323.15 K and at pressures from (10−70) MPa. Under these conditions, pure CO_2 is at a supercritical state. The results are given in Table S1 of the Supplementary Materials file. The experimental densities of carbon dioxide were compared with the values from the reference equation of state developed by Span and Wagner [35] with an estimated uncertainty, $U_c(\rho)$= 0.05 %. From this comparison, an Average Absolute Deviation (AAD% = $\text{abs}(\frac{1}{n}\sum_{i=1}^{n} 100 \times \frac{|x_i^{exp} - x_i^{EoS}|}{x_i^{EoS}})$) of 0.08 and a Maximum Deviation (MD % = $\max(100 \times \frac{|x_i^{exp} - x_i^{EoS}|}{x_i^{EoS}})$) of 0.21 at 313.15 K and an AAD % of 0.07 and a MD % of 0.22 at 323.15 K were observed. It should be noticed that the relative deviations increase as pressure decreases towards the critical pressure of CO_2, as shown in

Table 3
PC-SAFT[a] and SAFT-VR Mie[b] EoS parameters for pure carbon dioxide (CO_2), *n*-heptane (*n*-C_7), and *n*-dodecane (*n*-C_{12}) where m_s is the number of segments, σ is the diameter of the segment, ε is the strength of the interaction, and λ_r and λ_a are the repulsive and attractive exponents, respectively.

	PC-SAFT EoS			SAFT-VR Mie EoS				
Substance	m_s	$\sigma/Å$	$(\varepsilon/k)/K$	m_s	$\sigma/Å$	$(\varepsilon/k)/K$	λ_r	λ_a
CO_2	2.0729	2.7852	169.21	1.50	3.1916	231.88	27.557	5.1646
n-C_7	3.4831	3.8049	238.40	2.3949	4.4282	358.51	17.092	6.00
n-C_{12}	5.3060	3.8959	249.21	3.2519	4.7484	437.72	20.862	6.00

[a]From Gross and Sadowski [28], [b]From Lafitte et al.[11].

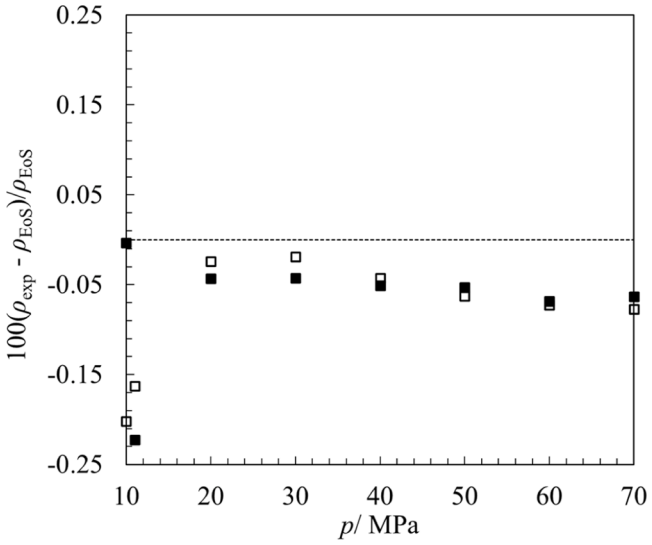

Fig. 3. Deviations between Span and Wagner EoS [26] and measured values for density of pure CO_2. □; (313.15 K) and ▌; (323.15 K).

Fig. 3. Across the range, experimental data show an underestimation of EoS as a reference. In this near critical domain, the density is lower (around 620 kg·m^{-3}) than at high pressure and the change in density with respect to pressure is significant, making the relative uncertainty in density caused by pressure uncertainty significant. Concerning experimental *n*-C_7 densities, a comparison was made with those from the Span and Wagner equation of state [36] ($U_c(\rho)$= 0.2 %), and good agreement was obtained for both temperatures, with an AAD of 0.03 % and an MD of 0.06 % at 313.15 K, and an AAD of 0.03 % and an MD of 0.05 % at 323.15 K. Similarly, the experimental density of *n*-C_{12} was compared with Lemmon and Huber EoS [37] ($U_c(\rho)$= 0.2 %), and an excellent match was obtained, particularly at 313.15 K and up to 50 MPa, with an AAD of 0.03 % and an MD of 0.05 %. Similar results were obtained at 323.15 K up to 70 MPa, with an AAD of 0.03 % and an MD of 0.05 %. The AAD % and MD % from reference EoS are shown in Table 4.

4.2. Binary systems

4.2.1. CO_2 + *n*-C_7

Herein, we present experimental densities of six mixtures of the CO_2 + *n*-C_7 binary system at 313.15 K and 323.15 K under eight different pressures. The CO_2 mole fraction in these mixtures was greater than 89 %, with pressures ranging from (10−70) MPa. Tables S2 and S5 in Supplementary Material lists the obtained densities for this binary system.

Table 4
Average Absolute Deviation percentages (AAD/%) and Maximum Deviation percentages (MD/%) from reference EoS.

	T = 313.15 K		T = 323.15 K		
Compound	AAD/%	MD/%	AAD/%	MD/%	Ref.
CO_2	0.08	0.21	0.07	0.22	[35]
n-C_7	0.03	0.06	0.03	0.05	[36]
n-C_{12}	0.03	0.05	0.03	0.05	[37]

Few density data of the CO_2 + *n*-C_7 mixture in the supercritical state is available in the literature. Fenghour et al. [38] reported density measurements for CO_2 + *n*-C_7 at temperatures from 302 K to 459 K and the pressure range from (3.61–55.48) MPa at three composition 29.18 %, 38.88 % and 42.70 % on molar fraction of CO_2. Medina-Bermudez et al. [39] reported experimental densities for this binary system at five compositions from 2.18 % to 94.96 % in a range of temperatures from 313.08 K to 362.38 K at several pressures up to 24.906 MPa. Bazile et al. [6] presented measurements for two isotherms: 303.35 K and 313.25 K over a range pressures from 10.12 MPa to 70.54 MPa. Unfortunately, they limited their study to mixtures containing up to 83.26 % carbon dioxide, making the investigation of the system at infinite dilution of *n*-C_7 in CO_2 difficult. Nevertheless, they used an extrapolation to study the volumetric properties of the system at infinite dilution focusing on the densities and derivatives properties such as partial molar volumes and excess isothermal compressibility.

We have determined the density of different mixtures with high CO_2 content to complement the work mentioned in [6]. The objective was to obtain an analytical equation that accurately represents the density as a function of CO_2 composition in the vicinity of infinite dilution. In Fig. 4, the mixture densities are plotted for all composition in the experimental pressure range for the CO_2 + *n*-C_7 mixture at 313.15 K. A clear inversion in the density trend with composition is observed around 15 MPa: at lower pressures, increasing the CO_2 content leads to a decrease in density, whereas at higher pressures, it leads to an increase. A similar behavior can be observed at 323.15 K, although in this case, the inversion occurs at a higher pressure of approximately 20 MPa.

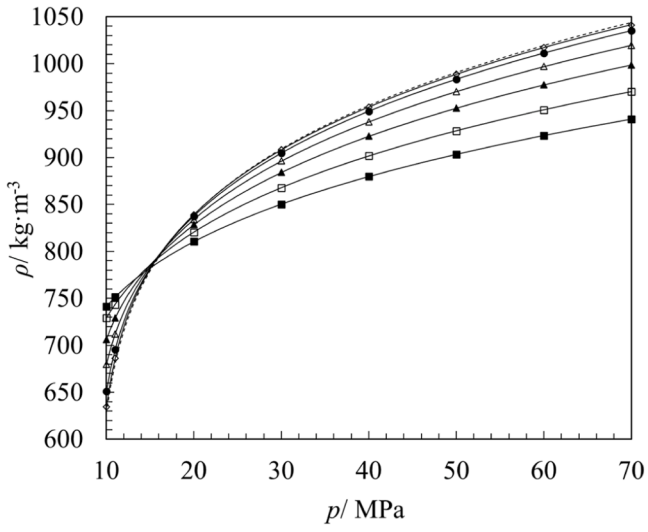

Fig. 4. Experimental densities of CO_2 + *n*-C_7 as a function of pressure for all compositions and pure CO_2 at 313.15 K, where; ■; (89.39 %), □; (93.00 %), ▲; (96.00 %), △; (98.00 %), ✦; (99.28 %), ✧; (99.79 %) and ——; (100 %) mol% CO_2. Lines are a guide for eyes.

4.2.2. $CO_2 + n\text{-}C_{12}$

For the binary mixture of $CO_2 + n\text{-}C_{12}$, density measurements were carried out at the same conditions of pressure and temperature as for $CO_2 + n\text{-}C_7$, with solvent compositions ranging from (90–99.5) mol% of CO_2. The results are reported in Tables S3 and S6 of the Supplementary Materials file.

This system has been previously studied by different authors. Ashcroft et al.[40] measured densities and computed derivatives properties such as partial molar volume, using a vibrating tube densitometer at a mole fraction gas solubility of 0.0129 under conditions of 298.15 K and a pressure of 0.1 MPa. Zhang et al.[41] measured densities at temperatures ranging from 313.55 K to 353.55 K at four different CO_2 molar percentages from 24.97 % to 86.10 %, and the density of $n\text{-}C_{12}$ under pressures, from 8 to 18 MPa. Zambrano et al.[42] reported density measurements and excess volume for this system in a range of temperatures from 283.15 K to 393.15 K with CO_2 content from 10.14 % to 60.22 % and pressures up to 100 MPa. Nevertheless, the experimental conditions including pressure, temperature, and composition did not align with those utilized in this present work, in particular regarding high CO_2 content above 90 mol%.

Bazile et al.[7] studied this mixture at eight different compositions of CO_2 ranging from 20.5 % to 98.77 % in molar percentages at two isotherms, 303.15 K and 313.15 K, and pressures ranging from (10−70) MPa. Fig. 5 shows the experimental densities of the $CO_2 + n\text{-}C_{12}$ system as a function of pressure at 323.15 K for all investigated compositions. In this system and at this temperature, a crossover point similar to that observed for the $CO_2 + n\text{-}C_7$ mixture appears around 20 MPa.

4.3. Ternary system

4.3.1. $CO_2 + n\text{-}C_7 + n\text{-}C_{12}$

The ternary system, composed of CO_2, $n\text{-}C_7$ and $n\text{-}C_{12}$, was analyzed as a pseudo-binary system comprising CO_2 and a hydrocarbon mixture to compare the results with those obtained on binary mixtures. Only one specific mole ratio between the two hydrocarbon component was considered, which is $x_{n-C_{12}}/x_{n-C_7} = 0.47$. In contrast, the CO_2 content in mixtures studied varied between 90 mol% and 100 mol%. In total, 6 ternary mixtures were investigated at the same pressure and temperature conditions as those of the binary systems. The obtained density data for these ternary mixtures are given in Tables S4 and S7 of the Supplementary Materials file. Santos et al. [43] measured the densities from 293.15 K to 363.15 K and for pressure up to 70 MPa in the ternary mixture $CO_2(1) + n\text{-}C_7(2) + n\text{-}C_{12}(3)$ at two compositions: 49.09 mol% and 74.25 mol% of CO_2. Unfortunately, the experimental conditions for the compositions of $n\text{-}C_7$ and $n\text{-}C_{12}$ in their ternary mixtures, using $x_2 = x_3 = (1 - x_1)/2$ do not precisely match those considered here and do not cover near-infinite dilution of hydrocarbons as studied here. In Fig. 6 experimental densities are plotted as a function of pressure at 313.15 K for all compositions studied with this ternary system. As noted with both binary systems at this temperature condition, for pressures ranging from 16 MPa to 70 MPa densities increase as CO_2 content increases below the density of pure CO_2. However, at pressures below 16 MPa, the reverse trend can be seen. As previously indicated, a small increase in solute amount results in a significant increase in the density of the system at the lowest pressures. This phenomenon is further illustrated in Fig. 7, where the density is presented as a function of mole fraction for different isobars at 323.15 K. It can be seen that isobars above 20 MPa display a monotonous increase, whereas those below 20 MPa show a regular decrease over the same composition range. At 20 MPa, the isobaric curve appears nearly horizontal, corresponding to the crossover point observed in the ρ–p diagram. It is important to note that the observation of a nearly horizontal isobaric curve is limited to the composition range between 0.90 and 1. Below this range, the curve is no longer flat, meaning that the impression of a sharp crossover observed in Figs. 4, 5 and 6 is also a consequence of the restricted composition window. When the composition range is extended, the isopleths still intersect, but no longer at a single point—rather, over a broader region. This indicates that the plateau observed in the ρ–x curve, or the crossover seen in the ρ–p diagram at a given temperature, does not correspond to the intersection of the pure-component isothermal density curves. That intersection occurs at a lower pressure, and thus at a lower density. Santos et al. [43] reported a similar trend for this ternary mixture at 363.15 K and 20 MPa.

4.4. SAFT modelling

Below we present the results of density modelling of the studied systems using the two EoSs described in Section 3. The predicted densities are found in Tables S1, S2, S3 and S4 and were compared with the experimental ones. The results of the comparison between experimental and calcualted data, in terms of AAD % and MD %, and optimized k_{ij} are listed in Table 5. For pure CO_2, PC-SAFT underestimates the density

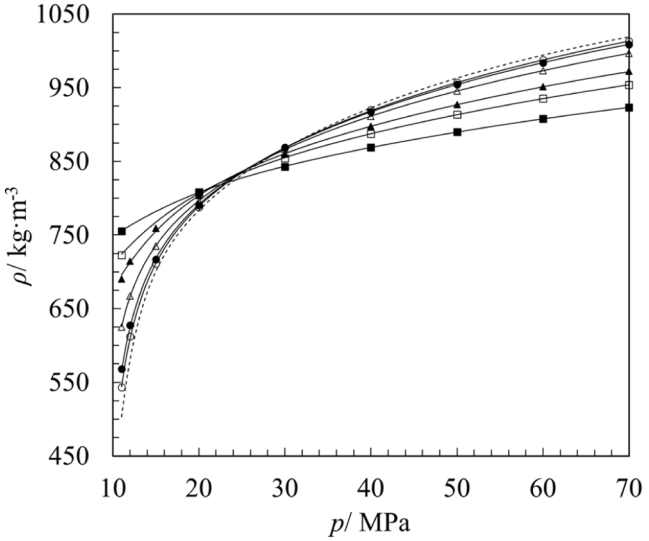

Fig. 5. Experimental densities of $CO_2 + n\text{-}C_{12}$ mixture as a function of pressure for all compositions and pure CO_2 at 323.15 K. ■; (90.00 %), □; (94.02 %), ●; (96.00 %), ○; (98.20 %), ▲; (99.20 %), △ (99.50 %) and ——; (100 %) mol% CO_2. Lines are a guide for eyes.

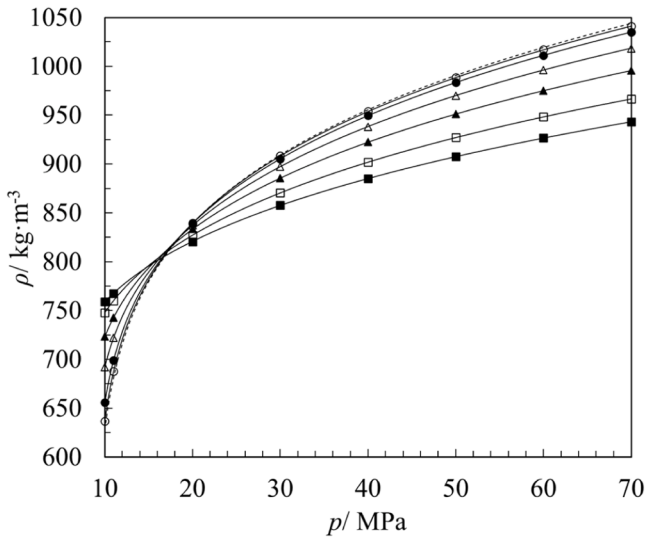

Fig. 6. Experimental densities of $CO_2 + n\text{-}C_7 + n\text{-}C_{12}$ as a function of pressure for all compositions and pure CO_2 at 313.15 K. ■; (90.00 %), □; (93.03 %), ▲; (96.00 %), △; (98.03 %), ●; (99.30 %), ○; (99.80 %), and ——; (100 %) mol% CO_2. Lines are a guide for eyes.

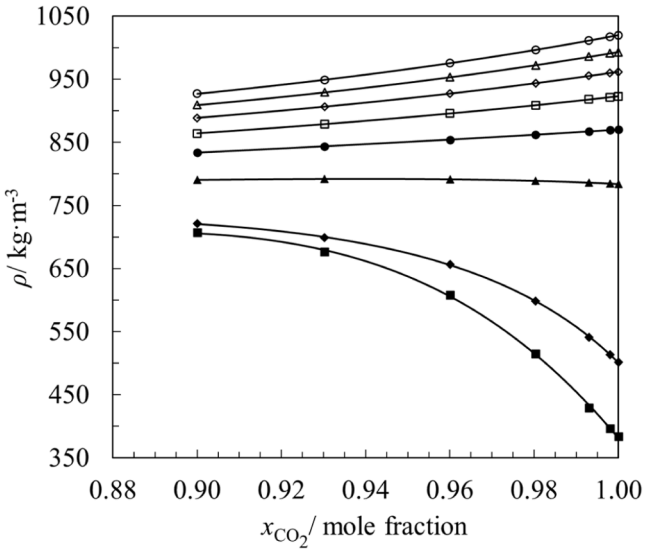

Fig. 7. Experimental densities of CO_2 + n-C_7 + n-C_{12} as a function of molar fraction of CO_2 from 10 to 70 MPa at 323.15 K. ■; (10 MPa), ◆; (11 MPa), ▲; (20 MPa), ● (30 MPa), □; (40 MPa), ◊ (50 MPa), △; (60 MPa) and ○; (70 MPa). Lines are a guide for eyes.

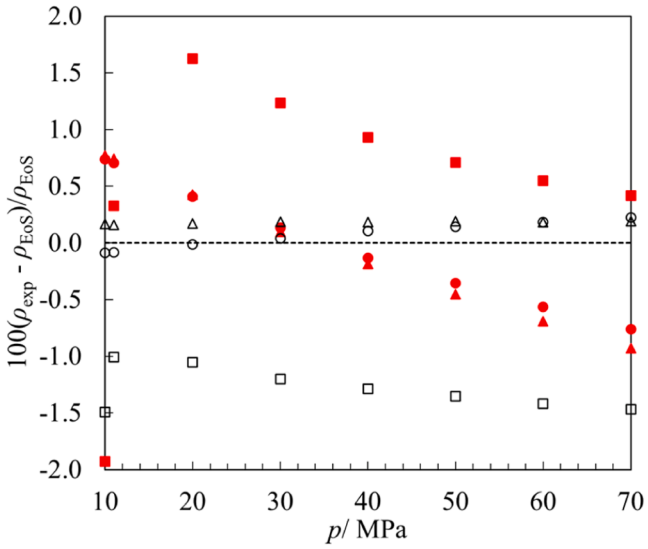

Fig. 8. Deviations from PC-SAFT and SAFT-VR Mie EoS density predictions at 313.15 K over all experimental pressures. ■ □; (pure CO_2), ● ○; (pure n-C_7) and ▲△; (pure n-C_{12}). Filled symbols (PC-SAFT), empty symbols (SAFT-VR Mie).

Table 5
Binary interaction parameter (k_{ij}) and comparison between experimental and calculated densities in terms of average absolute deviation (AAD/%)[a] and maximum deviation (MD/%)[b].

		PC-SAFT EoS			SAFT-VR Mie EoS		
System	T/K	k_{ij}	AAD/ %	MD/ %	k_{ij}	AAD/ %	MD/ %
CO_2	313.15	-	0.96	1.98	-	1.29	1.51
	323.15	-	2.27	7.73	-	1.79	3.53
n-C_7	313.15	-	0.47	0.76	-	0.11	0.22
	323.15	-	0.47	0.78	-	0.11	0.21
n-C_{12}	313.15	-	0.54	0.91	-	0.16	0.17
	323.15	-	0.53	0.91	-	0.15	0.17
CO_2 + n-C_7	313.15	0	2.65	8.62	0	1.57	5.79
	313.15	0.120	0.72	1.68	0.053	0.79	1.46
	323.15	0	4.40	20.30	0	2.16	11.24
	323.15	0.120	1.49	8.75	0.053	1.23	3.89
CO_2 + n-C_{12}	313.15	0	3.02	8.77	0	1.45	4.50
	313.15	0.125	0.66	1.52	0.057	0.86	1.45
	323.15	0	4.31	20.48	0	1.39	6.41
	323.15	0.125	0.97	4.52	0.057	1.38	3.95
CO_2 + n-C_7 + n-C_{12}	313.15	0.120 / 0.125	0.65	1.64	0.055	0.80	1.48
	323.15	0.120 / 0.125	1.54	9.70	0.055	1.27	3.68

[a]AAD (%) = Average Absolute Deviation; [b]MD (%) = Maximum Deviation Percentages.

value at both temperatures, except for the lowest pressure. The largest deviations are obtained in the region in which the density change with pressure is most pronounced, close to 9.0 MPa at 313.15 K and 10.4 MPa at 323.15 K [35]. On the other hand, SAFT-VR Mie overestimated the densities at all pressures and temperatures. This EoS predicted the density better than the other one with smaller deviations, especially at 323.15 K. For n-C_7 and n-C_{12}, the results obtained with SAFT-VR Mie were somewhat better than PC-SAFT ones (Table S1). The experimental conditions were far from the critical conditions of these compounds so the deviations were similar along p and T as shown in Fig. 8.

For binary mixtures, initial calculations with k_{ij}= 0 were performed. Both equations of state correctly predict the non-ideal behaviors of the systems, i.e., the strong density increase with solute content at the lowest pressure. For all mixtures, introducing nonzero k_{ij} significantly improved the predictive accuracy of both SAFT models. In the case of PC-SAFT, at 313.15 K, the AAD % was reduced to 0.72 % for the CO_2 + n-C_7 and to 0.66 % for CO_2 + n-C_{12}. Similarly, for SAFT-VR Mie, the AAD % for CO_2 + n-C_7 decreased from 1.57 % to 0.79 %. Therefore, both EoS have improved their predictive accuracy by adding the binary interaction parameter.

To assess the performance of the two equations of state using optimized binary interaction parameters, calculated densities were compared in Figs. 9 to 11 with experimental data. Fig. 9 shows density as a function of pressure along various isopleths for the CO_2–n-C_7 binary mixture at 323.15 K. Fig. 10 presents density versus CO_2 mol% along different isobars for the CO_2–n-C_{12} binary system at 313.15 K. Finally, Fig. 11 illustrates the same property for the ternary mixture as a function of composition at 313.15 K and various isobars. In all cases, the models capture the influence of pressure and CO_2 composition with good accuracy for both binary and ternary mixtures. The deviations observed

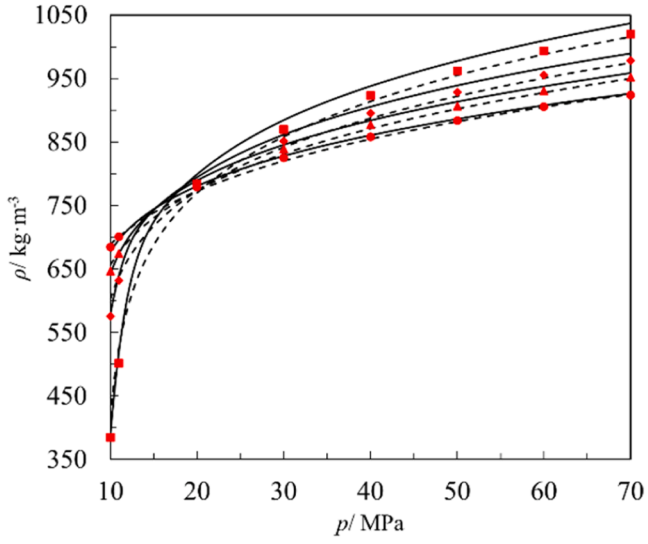

Fig. 9. Density predictions using PC-SAFT and SAFT-VR Mie EoS as a function of pressure at 323.15 K for the CO_2 + n-C_7 binary mixture. —; (PC-SAFT),–; (SAFT-VR Mie), data: ●; (89.39 %), ▲; (93 %), ♦; (96 %), and ■ (100 %) mol % CO_2.

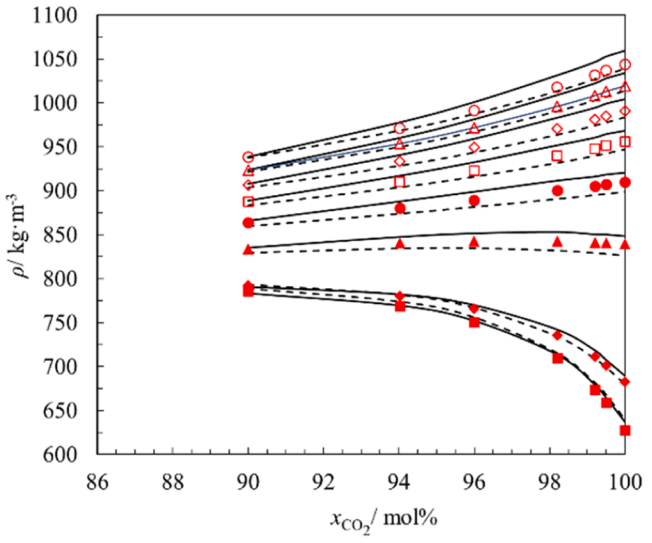

Fig. 10. Density predictions as a function of pressure from PC-SAFT and SAFT-VR Mie EoS at 313.15 K for the CO_2 + *n*-C_{12} binary mixture. —; (PC-SAFT),–; (SAFT-VR Mie), data: ■; (10 MPa), ♦; (11 MPa), ▲; (20 MPa), ●; (30 MPa), □; (40 MPa), ◊; (50 MPa), △; (60 MPa) and ○; (70 MPa).

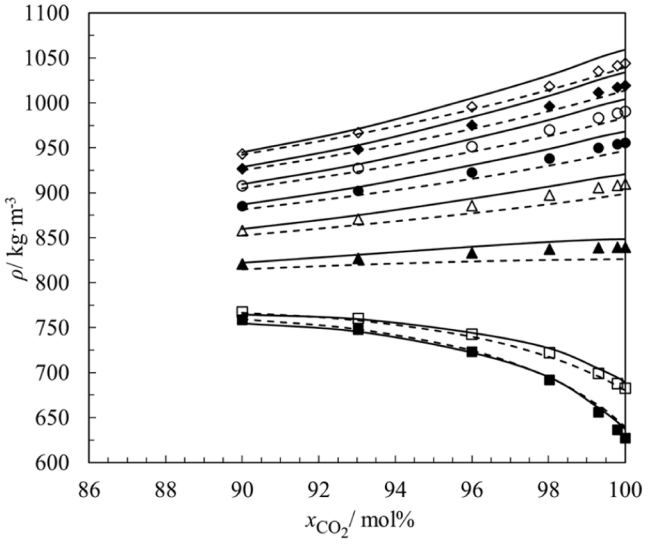

Fig. 11. Density predictions as a function of pressure from PC-SAFT and SAFT-VR Mie EoS at 313.15 K for the CO_2 + *n*-C_7 + *n*-C_{12} ternary mixture. —; (PC-SAFT),–; (SAFT-VR Mie), data: ■; (10 MPa), □; (11 MPa), ▲; (20 MPa), △; (30 MPa), ●; (40 MPa), ○; (50 MPa), ◆; (60 MPa) and ◄; (70 MPa).

between calculated and experimental data mainly result from the inability of the equation of state to reproduce the density of pure CO_2 with the unmodified pure-component parameters. Both equations of state show similar absolute deviations; however, SAFT-VR tends to systematically overestimate densities, while PC-SAFT consistently underestimates them relative to experimental values. Nevertheless, the smaller values of k_{ij} for SAFT-VR Mie, indicated that it is a better predictive model than PC-SAFT for our asymmetric systems. The calculated values of the density of the three systems at 313.15 K are reported in Tables S2, S3, and **S4** given in the Supplementary Material. Additionally, Tables S5, S6, and **S7** of the Supplementary Materials file list the predicted densities at 323.15 K, which are compared with the experimental values.

5. Derivatives properties

5.1. Partial Molar Volume (PMV)

The calculation of properties derived from experimental densities of mixtures provides insights into the nature of solute-solvent interactions. The discussion is especially interesting if the composition of the mixtures corresponds to infinite dilution conditions as in this work. This section analyzes the partial molar volume of a component *i* (v_i) and the cluster size of the binary and ternary mixtures. The calculation was performed at (10, 11, and 20) MPa, and at 313.15 K and 323.15 K. The v_i is an intensive property that is influenced by pressure, temperature, and composition. When the partial molar volume of a component differs significantly from its pure molar volume, it indicates that the solution exhibits non-ideal behavior, which can be due to factors such as solvation or clustering effects. For a solute, the disparity between the partial molar volume and its molar volume in the pure state becomes often increasingly more pronounced as solute composition approaches infinite dilution due to the solvent environnement. Thus, analyzing partial molar volumes of a solute at infinite dilution $v^{\infty}_{\text{solute}}$ can provide insights into the nature and extent of the deviations to ideal solution behavior. For the CO_2 + *n*-C_x binary system, the partial molar volumes were determined using the following relations:

$$v_{CO_2} = V_m + (1 - x_{CO_2})\left(\frac{dV_m}{dx_{CO_2}}\right)_{p,T} \tag{8}$$

$$v_{n-C_x} = V_m - x_{CO_2}\left(\frac{dV_m}{dx_{CO_2}}\right)_{p,T} \tag{9}$$

Those equations relate the v_i to the molar volume of the mixture (V_m) and its derivative with respect to CO_2 molar fraction at constant pressure and temperature $(dV_m/dx_{CO_2})_{p,T}$. This latter was calculated using a curve-fitting method, which first involves fitting the experimental density data as a function of the molar fraction x_{CO_2}, followed by an analytical differentiation of the resulting function. Since there is no theoretical function to describe $\rho(x_{CO_2})$, an empirical function must be selected for the fitting process. The choice of the functional form is crucial not only for achieving a good fit but, more importantly, for ensuring the appropriateness of the derivative calculation, particularly at the boundary of the domain, i.e. at $x_{CO_2} = 1$. The lack of a theoretical form makes the estimation of the uncertainty in the calculated derivative challenging. To address this, two types of functions were tested to guide the selection process: polynomial and Padé-type approximations. The latter is expressed as the ratio of two polynomials of degrees *M* and *N*, and can be written as:

$$\text{Padé } [M/N] = \frac{\sum_{i=0}^{M} a_i \rho^M}{1 + \sum_{j=1}^{N} b_j \rho^N} \tag{10}$$

where a_i and b_j are the fitted parameters. To achieve this, Python programming code was written using libraries such as NumPy, Pandas, and SciPy. The code employs a curve-fitting approach to identify the most accurate mathematical model representing the relationship between the mole fraction of CO_2 and the density of a mixture. A suite of mathematical functions is tested using a non-linear least-squares minimization algorithm (the `curve_fit` function from the `scipy.optimize` module) to identify optimal parameters. The objective function used by `curve_fit` is the sum of squared residuals ($\sum_{i=0}^{n}\left(\rho^{i}_{calc} - \rho^{i}_{exp}\right)^2$), which is minimized to determine the best-fit parameters for each function. The code then calculates deviations, such as the AAD % and MD %, to assess the accuracy of each function. This approach enables the selection of the function that best captures the experimental data, providing a robust and reliable representation of the relationship between the mole fraction of CO_2 and density. Table S8 of the

Supplementary Materials file provides a list of the tested functions including their forms and the observed deviations from experimental data. For both Padé-type and polynomial approximations, increasing the degree (parameters) in the equations above a certain value does not significantly improve the fit, as it may lead to overfitting of the experimental data, resulting in poor data smoothing and potentially increasing errors in the derivation(Fig. 12). Therefore, the tests were limited to fourth degree in both polynomial and Padé-type functions. Among all tested functions, we chose the Padé [2/4] equation with four parameters was chosen for the computation. This approach not only provides a good fit to the experimental data but also smooths the data up to infinite dilution. To assess the uncertainty in dV_m/dx_{CO_2}, a pseudo-random perturbation of the density data was conducted using 5000 trials. From this analysis, we determined v_{CO_2}, v_{n-C_x}, and the corresponding combined uncertainties (Table S9 in Supplementary Material).

The partial molar volumes of solutes obtained for both binary mixtures are plotted as a function of mole fraction for (10, 11 and 20) MPa isobars at 313.15 K in Fig. 13. For the (10 and 11) MPa isobars, it is noticed a change in sign from positive towards negative values as CO_2 content increases. Negative solute PMV values at infinite dilution in supercritical CO_2 were previously reported both experimentally [6,12, 44–46] and from molecular simulations [13]. A negative value for the PMV of solute at infinite dilution indicates that the addition of solute to a mixture enclosed in a fixed volume V results in a pressure drop corresponding to a negative derivative of pressure with respect to addition of solute moles:

$$\left(\frac{\partial p}{\partial n_{\text{solute}}}\right)_{T,V} = -\frac{v_{\text{solute}}}{\left(\frac{\partial n V_m}{\partial p}\right)_{T,n}} < 0 \tag{11}$$

As shown in Fig. 14 for the binary mixture of CO_2 + n-C_7 at 313.15 K and 10 MPa, the decline in solute PMV implies a crossover regarding the PMVs of the solvent and solute, indicating that they are equal at the crossover composition. Therefore, at this specific composition, the molar volume V_m is also equal to both PMVs due to the following relationship:

$$V_m = x_{CO_2} v_{CO_2} + (1 - x_{CO_2}) v_{\text{solute}} = v_{CO_2} \tag{12}$$

Furthermore, at this specific point, the molar volume reaches a minimum as its derivative with respect to mole fraction equals zero according to:

$$\left(\frac{\partial V_m}{\partial x_{CO_2}}\right)_{p,T} = \frac{v_{CO_2} - V_m}{1 - x_{CO_2}} = 0 \tag{13}$$

The observation of a negative PMV at infinite dilution in the CO_2 + solute system, leading to contraction of the system upon the addition of solute particules in pure CO_2 near critical condition, can be attributed to a clustering effect. Eckert et al.[44] defined this effect as the

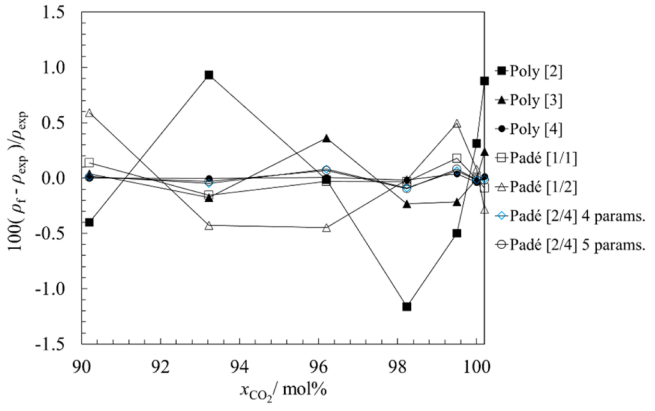

Fig. 12. Deviations from the experimental data for each tested function for the ternary mixture at various CO_2 molar percentages at 10 MPa and 313.15 K.

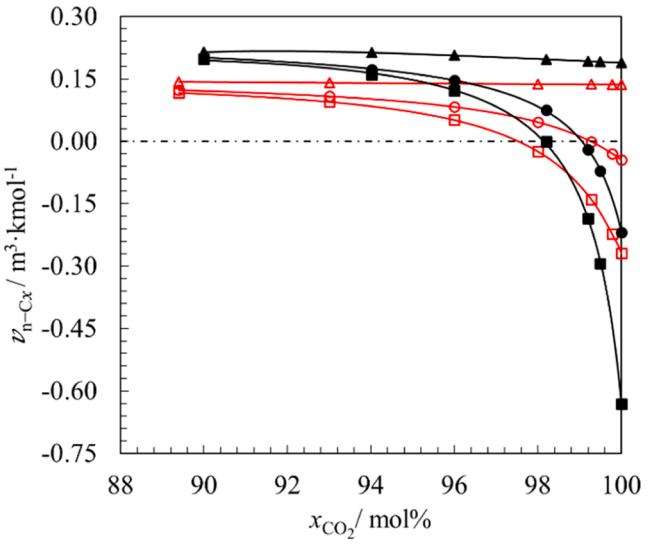

Fig. 13. Partial molar volumes of alkanes for binary mixtures as a function of CO_2 molar percentages at 313.15 K. Square □; (10 MPa), circle ○; (11 MPa), and triangle △; (20 MPa). Red lines represent the partial molar volume of n-C_7, and black lines represent the partial molar volume of n-C_{12}.

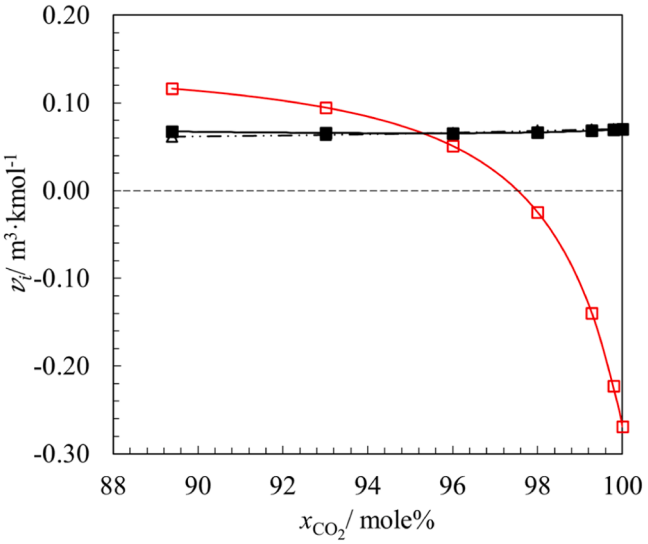

Fig. 14. Partial molar volumes of n-C_7 for the binary mixtures as a function of CO_2 molar percentages at 313.15 K and 10 MPa. The red line represents the partial molar volume of n-C_7, the solid black line represents the partial molar volume of CO_2, and the dotted line represents the molar volume of the binary mixture.

phenomenon where solvent molecules aggregates around solute molecules upon the addition of solute particles in the system. Debenedetti et al.[12] concluded that the link between the clustering effect and the change of PMV occurs near the critical point of the solvent. Therefore, measuring volumetric properties measurements at near-infinite dilution near the critical point of solvent becomes essential for identifying the conditions where clustering phenomena becomes significant, helping to define process conditions.

The magnitude of this clustering effect can be quantified using the cluster size ξ_{cluster}, which represents the excess number solvent molecules surrounding a single solute molecule at infinite dilution. Based on the statistical mechanical theory of solutions by Kirkwood and Buff [47], ξ_{cluster} can be estimated from the following relation [12]:

$$\xi_{\text{cluster}} = \frac{RT\kappa_{T,CO_2} - v^{\infty}_{\text{solute}}}{V_{m,CO_2}} \quad (14)$$

where κ_{T,CO_2} and V_{m,CO_2} are the isothermal compressibility and molar volume of pure CO_2. For both CO_2 + n-C_7 and CO_2 + n-C_{12} mixtures, the solute partial molar volume becomes negative at high concentrations of CO_2 below 20 MPa and both experimental temperatures (313.15 K and 323.15 K), indicating the formation of clusters in this pT range (Table 6). Conversely, at 20 MPa and above, both partial molar volumes are positive, leading to a negative value for ξ_{cluster}, with the partial molar volume of n-C_7 having values higher than that of CO_2. Debenedetti et al. [12] mentioned that negative values of ξ_{cluster} (positive partial molar volume) correspond to a physical sense of repulsion. It should be emphasized that neither the crossover of partial molar volume curves shown in Fig. 14 nor the clustering phenomenon is directly related to the intersection of density isopleths, as observed in Figs. 4, 5 and 6. These are fundamentally distinct properties. A crossover between density isopleths may occur without the presence of clustering, as illustrated by the CO_2–n-C_7 system at 303.15 K [6]. Conversely, clustering should arise even in the absence of any isopleth intersection, particularly when the solute has a density that is either consistently higher or consistently lower than that of CO_2 across the full pressure range. To investigate this behavior experimentally and by molecular simulation, binary systems involving either very light or very heavy solutes mixed with CO_2 are planned for study in the next phase of our research program.

The same procedure for calculating the PMV was applied to the ternary mixture, by treating it as a pseudo-binary mixture. As for binary mixtures, the results show that PMV values below 20 MPa are negative, indicating a clustering phenomenon at both temperatures. Interestingly, it has been noticed that the clustering effect in this ternary mixture treated as a pseudo-binary is linearly correlated with that observed in the binary mixtures, following the relationship $\xi^{\text{pseudo-binary}}_{\text{cluster}} = f(x_{n-C_7}, x_{n-C_{12}})$, as shown in Table 6 and Fig. 15. This important result suggests that the clustering effect may be additive in mixtures containing different solutes and could be estimated using a simple mole-fraction-weighted average based on the corresponding binary mixtures. In other words, it indicates that the mixture behaves as an ideal solution of clusters in a supercritical solvent. However, a more extensive analysis of other CO_2 + alkane systems is necessary to confirm this general linear correlation.

6. Conclusion

This work provides a comprehensive study of density and clustering phenomena in binary and ternary CO_2-rich systems containing n-heptane (n-C_7) and n-dodecane (n-C_{12}) under supercritical conditions. Density measurements were performed with high precision using a modified vibrating U-tube densimeter, with a new protocol enabling analysis of systems with CO_2 compositions between (90 and 99.8) mol% across a pressure range of (10−70) MPa and temperatures of 313.15 K and 323.15 K.

The experimental results show a significant deviation from ideal solution behavior in these mixtures, especially at pressures below 20 MPa. For these conditions, partial molar volumes of the hydrocarbons exhibited negative values, indicating contraction of the system up addition of hydrocarbon solute molecules into the CO_2 solvent due to clustering. This clustering effect becomes more prominent near the CO_2 critical point, where solvent compressibility is highest. These findings support the hypothesis that the addition of solute molecules under supercritical conditions leads to the formation of solute-solvent aggregates, as defined by the clustering phenomenon.

Table 6
Cluster sizes (ξ_{cluster}) for all mixtures at the pressures and temperatures studied.

System	313.15 K			323.15 K		
	10 MPa	11 MPa	20 MPa	10 MPa	11 MPa	20 MPa
CO_2 + n-C_7	8	3	< 0	22	15	< 0
CO_2 + n-C_{12}	13	6	< 0	32	24	< 0
CO_2 + n-C_7 + n-C_{12}	10	4	< 0	27	17	< 0

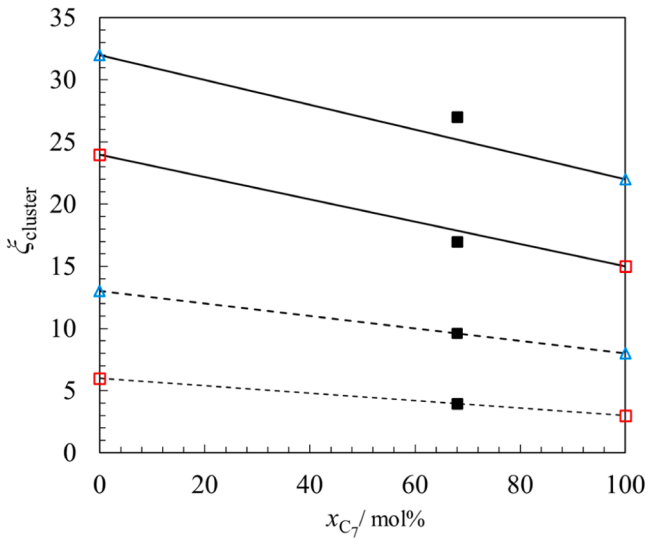

Fig. 15. Linear correlation between the cluster size ξ_{cluster} and n-C_7 composition. △; p = 10 MPa, □; p = 11 MPa. —; T = 313.15 K, –; T = 323.15 K. ■; $\xi^{\text{pseudo-binary}}_{\text{cluster}} = f(x_{n-C_7}, x_{n-C_{12}})$ on the ternary mixture.

For the ternary mixture (CO_2 + n-C_7 + n-C_{12}), treated as a pseudo-binary system, the clustering behavior appeared to be additive. The cluster size in the ternary system showed a linear trend consistent with those observed in the corresponding binary mixtures, suggesting that clustering in multicomponent systems may be estimated using a simple mole-fraction-weighted average. These findings point to the potential for simplifying the description of complex CO_2–hydrocarbon mixtures in supercritical applications. Nevertheless, further measurements involving CO_2 + alkane systems are needed to confirm the general applicability of this linear behavior.

The study further evaluated the predictive capabilities of two SAFT-type equations of state, PC-SAFT and SAFT-VR Mie, in reproducing the observed experimental behavior. While both models effectively captured the non-ideal trends and density variations at high solute dilution, they exhibited notable deviations near the CO_2 critical point. The introduction of optimized binary interaction parameters (BIPs) significantly improved predictive accuracy, reducing deviations for both binary and ternary systems. However, the challenges observed near critical conditions underscore the need for further refinement of these models to accurately describe density and clustering phenomena.

Overall, this study provides new insights into the volumetric properties, clustering mechanisms, and additivity of clustering effects in CO_2-rich systems under supercritical conditions. These findings have significant implications for industrial processes utilizing supercritical CO_2, such as supercritical fluid extraction, enhanced oil recovery, and carbon capture and storage, where understanding solute-solvent interactions and predicting volumetric behavior are critical for process optimization. Future work will focus on validating these results through molecular simulations and extending the analysis to other solutes and multicomponent systems.

CRediT authorship contribution statement

Manuela Artal: Writing – review & editing, Validation, Supervision, Methodology, Conceptualization. **Ariel A. Acuña:** Writing – original draft, Software, Investigation, Conceptualization. **Daridon jean luc:**

Writing – review & editing, Validation, Supervision, Methodology, Conceptualization. **Guillaume Galliero:** Writing – review & editing, Validation, Supervision, Methodology, Conceptualization.

Declaration of Competing Interest

The authors declare that they have no known competing financial interests or personal relationships that could have appeared to influence the work reported in this paper.

Acknowledgements

We are grateful to “Cotutelles transfrontalières UPPA\UNIZAR” program for the phD grant allowed to Ariel A. Acuña. We would like to thank Pau University and Zaragoza University for providing the necessary facilities and technical support. We also gratefully acknowledge Dr. Bell Ian for his insightful discussions and valuable assistance with data analysis and interpretation of the results.

Appendix A. Supporting information

Supplementary data associated with this article can be found in the online version at doi:10.1016/j.supflu.2025.106778.

Data availability

Data will be made available on request.

References

[1] C. Campalani, E. Amadio, S. Zanini, S. Dall'Acqua, M. Panozzo, S. Ferrari, G. De Nadai, S. Francescato, M. Selva, A. Perosa, Supercritical CO2 as a Green solvent for the circular economy: extraction of fatty acids from fruit pomace, J. CO2 Util. 41 (2020) 101259, https://doi.org/10.1016/j.jcou.2020.101259.
[2] S.K. Prasad, J.S. Sangwai, H.-S. Byun, A review of the supercritical CO2 fluid applications for improved oil and gas production and associated carbon storage, J. CO2 Util. 72 (2023) 102479, https://doi.org/10.1016/j.jcou.2023.102479.
[3] B. Dziejarski, R. Krzyżyńska, K. Andersson, Current status of carbon capture, utilization, and storage technologies in the global economy: a survey of technical assessment, Fuel 342 (2023) 127776, https://doi.org/10.1016/j.fuel.2023.127776.
[4] T. Wu, B. Han, Supercritical Carbon Dioxide (CO2) as Green Solvent, Supercrit. Carbon Dioxide (n.d.).
[5] C.B. Mehr, H.D. Cochran, Supercritical carbon dioxide extraction of caffeine from guaranh, J. Supercrit. Fluids 9 (1996).
[6] J.-P. Bazile, D. Nasri, A.W. Saley Hamani, G. Galliero, J.-L. Daridon, Excess volume, isothermal compressibility, isentropic compressibility and speed of sound of carbon dioxide + n-heptane binary mixture under pressure up to 70 MPa. I experimental measurements, J. Supercrit. Fluids 140 (2018) 218–232, https://doi.org/10.1016/j.supflu.2018.05.028.
[7] J.-P. Bazile, D. Nasri, A.W. Saley Hamani, G. Galliero, J.-L. Daridon, Density, speed of sound, compressibility, and excess properties of carbon dioxide + n -Dodecane binary mixtures from 10 to 70 MPa, J. Chem. Eng. Data 64 (2019) 3187–3204, https://doi.org/10.1021/acs.jced.9b00311.
[8] J.-L. Daridon, F. Montel, D.V. Nichita, J. Pauly, Fluid-fluid and fluid-solid phase equilibria in carbon dioxide + waxy systems 1. Co + n-C, Fluid Phase Equilibria 538 (2021) 113023, https://doi.org/10.1016/j.fluid.2021.113023.
[9] J.-P. Bazile, D. Nasri, G. Galliero, J.-L. Daridon, Density, speed of sound, compressibility, and excess properties in a carbon dioxide + n-Docosane binary mixture from 10 to 70 MPa, J. Chem. Eng. Data 67 (2022) 3374–3384, https://doi.org/10.1021/acs.jced.2c00472.
[10] W.G. Chapman, K.E. Gubbins, G. Jackson, M. Radosz, SAFT: Equation-of-state solution model for associating fluids, Fluid Phase Equilibria 52 (1989) 31–38, https://doi.org/10.1016/0378-3812(89)80308-5.
[11] T. Lafitte, A. Apostolakou, C. Avendaño, A. Galindo, C.S. Adjiman, E.A. Müller, G. Jackson, Accurate statistical associating fluid theory for chain molecules formed from mie segments, J. Chem. Phys. 139 (2013) 154504, https://doi.org/10.1063/1.4819786.
[12] P.G. Debenedetti, Clustering in dilute, binary supercritical mixtures: a fluctuation analysis, Chem. Eng. Sci. 42 (1987) 2203–2212, https://doi.org/10.1016/0009-2509(87)85042-X.
[13] S. Hamani, H. Hoang, T.Q.Q. Viet, J.-L. Daridon, G. Galliero, Excess volume, isothermal compressibility, isentropic compressibility and speed of sound of carbon dioxide+n-heptane binary mixture under pressure up to 70 MPa. II. Molecular simulations, J. Supercrit. Fluids 164 (2020) 104890, https://doi.org/10.1016/j.supflu.2020.104890.
[14] R.D. Chirico, M. Frenkel, J.W. Magee, V. Diky, C.D. Muzny, A.F. Kazakov, K. Kroenlein, I. Abdulagatov, G.R. Hardin, W.E. Acree, J.F. Brenneke, P.L. Brown, P.T. Cummings, T.W. De Loos, D.G. Friend, A.R.H. Goodwin, L.D. Hansen, W. M. Haynes, N. Koga, A. Mandelis, K.N. Marsh, P.M. Mathias, C. McCabe, J. P. O'Connell, A. Pádua, V. Rives, C. Schick, J.P.M. Trusler, S. Vyazovkin, R.D. Weir, J. Wu, Improvement of quality in publication of experimental thermophysical property data: challenges, assessment tools, global implementation, and online support, J. Chem. Eng. Data 58 (2013) 2699–2716, https://doi.org/10.1021/je400569s.
[15] H. Kalra, H. Kubota, D.B. Robinson, H.-J. Ng, Equilibrium phase properties of the carbon dioxide-n-heptane system, J. Chem. Eng. Data 23 (1978) 317–321, https://doi.org/10.1021/je60079a016.
[16] T.L. Chester, B.S. Haynes, Estimation of pressure-temperature critical loci of CO2 binary mixtures with methyl-*tert*-butyl ether, ethyl acetate, methyl-ethyl ketone, dioxane and decane, J. Supercrit. Fluids 11 (1997) 15–20, https://doi.org/10.1016/S0896-8446(97)00034-X.
[17] E.-J. Choi, S.-D. Yeo, Critical properties for carbon dioxide + n -Alkane mixtures using a Variable-Volume view cell, J. Chem. Eng. Data 43 (1998) 714–716, https://doi.org/10.1021/je9800297.
[18] M. Cismondi, S.B. Rodríguez-Reartes, J.M. Milanesio, M.S. Zabaloy, Phase equilibria of CO_2 + n -Alkane binary systems in wide ranges of conditions: development of predictive correlations based on cubic mixing rules, Ind. Eng. Chem. Res. 51 (2012) 6232–6250, https://doi.org/10.1021/ie2018806.
[19] L.E. Camacho-Camacho, L.A. Galicia-Luna, O. Elizalde-Solis, Vapor–Liquid equilibria of binary and ternary systems containing carbon dioxide, alkane, and benzothiophene, J. Chem. Eng. Data 56 (2011) 4109–4115, https://doi.org/10.1021/je200586g.
[20] J.-N. Jaubert, F. Mutelet, VLE predictions with the Peng–Robinson equation of state and temperature dependent kij calculated through a group contribution method, Fluid Phase Equilibria (2004).
[21] J.-P. Bazile, J.-L. Daridon, J.-N. Jaubert, K. Abou-Alfa, S. Vitu, Phase behavior of CO2 + 2,2-dimethylbutane and CO2 + 2-methylpentane from 293 k to 363 k and at pressures up to 11 MPa, Int. J. Thermophys. 46 (2025) 107, https://doi.org/10.1007/s10765-025-03579-5.
[22] S. Zid, J.-P. Bazile, J.-L. Daridon, A. Piña-Martinez, J.-N. Jaubert, S. Vitu, Fluid phase equilibria for the CO2 + 2,3-dimethylbutane binary system from 291.9 k to 373.1 k, J. Supercrit. Fluids 179 (2022) 105387, https://doi.org/10.1016/j.supflu.2021.105387.
[23] E.F. May, W.J. Tay, M. Nania, A. Aleji, S. Al-Ghafri, J.P. Martin Trusler, Erratum: “Physical apparatus parameters and model for vibrating tube densimeters at pressures to 140 MPa and temperatures to 473 K” [Rev. Sci. Instrum. 85, 095111 (2014)], Rev. Sci. Instrum. 86 (2015) 049902, https://doi.org/10.1063/1.4919437.
[24] E.F. May, W.J. Tay, M. Nania, A. Aleji, S. Al-Ghafri, J.P. Martin Trusler, Physical apparatus parameters and model for vibrating tube densimeters at pressures to 140 MPa and temperatures to 473 k, Rev. Sci. Instrum. 85 (2014) 095111, https://doi.org/10.1063/1.4894469.
[25] R. Span, E.W. Lemmon, R.T. Jacobsen, W. Wagner, A. Yokozeki, A reference equation of state for the thermodynamic properties of nitrogen for temperatures from 63.151 to 1000 k and pressures to 2200 MPa, J. Phys. Chem. Ref. Data 29 (2000) 1361–1433, https://doi.org/10.1063/1.1349047.
[26] W. Wagner, A. Pruß, The IAPWS formulation 1995 for the thermodynamic properties of ordinary water substance for general and scientific use, J. Phys. Chem. Ref. Data 31 (2002) 387–535, https://doi.org/10.1063/1.1461829.
[27] J.-L. Daridon, J.-P. Bazile, Computation of liquid isothermal compressibility from density measurements: an application to toluene, J. Chem. Eng. Data 63 (2018) 2162–2178, https://doi.org/10.1021/acs.jced.8b00148.
[28] J. Gross, G. Sadowski, Perturbed-Chain SAFT: an equation of state based on a perturbation theory for chain molecules, Ind. Eng. Chem. Res. 40 (2001) 1244–1260, https://doi.org/10.1021/ie0003887.
[29] M.S. Wertheim, Fluids with highly directional attractive forces. I. statistical thermodynamics, J. Stat. Phys. 35 (1984) 19–34, https://doi.org/10.1007/BF01017362.
[30] S.S. Chen, A. Kreglewski, Applications of the augmented van der waals theory of fluids.: I. Pure fluids, Ber. Bunsenges. F. üR. Phys. Chem. 81 (1977) 1048–1052, https://doi.org/10.1002/bbpc.19770811037.
[31] T. Laursen, VLXE - Advanced PVT Simplified, VLXE - Adv. PVT Simpl. (n.d.). ⟨http://www.vlxe.com⟩.
[32] I.H. Bell, U.K. Deiters, A.M.M. Leal, Implementing an equation of state without derivatives: teqp, Ind. Eng. Chem. Res. 61 (2022) 6010–6027, https://doi.org/10.1021/acs.iecr.2c00237.
[33] J.A. Barker, D. Henderson, Perturbation theory and equation of state for fluids. Ii. a successful theory of liquids, J. Chem. Phys. 47 (1967) 4714–4721, https://doi.org/10.1063/1.1701689.
[34] H. Hoang, S. Delage-Santacreu, G. Galliero, Simultaneous description of equilibrium, interfacial, and transport properties of fluids using a mie chain Coarse-Grained force field, Ind. Eng. Chem. Res. 56 (2017) 9213–9226, https://doi.org/10.1021/acs.iecr.7b01397.
[35] R. Span, W. Wagner, A new equation of state for carbon dioxide covering the fluid region from the Triple-Point temperature to 1100 k at pressures up to 800 MPa, J. Phys. Chem. Ref. Data 25 (1996) 1509–1596, https://doi.org/10.1063/1.555991.
[36] R. Span, W. Wagner, Equations of State for Technical Applications. II. Results for Nonpolar Fluids, (n.d.). https://doi.org/10.1023/A:1022310214958.
[37] E.W. Lemmon, M.L. Huber, Thermodynamic properties of n-Dodecane, Energy Fuels 18 (2004) 960–967, https://doi.org/10.1021/ef0341062.

[38] A. Fenghour, J.P.M. Trusler, W.A. Wakeham, Densities and bubble points of binary mixtures of carbon dioxide and n-heptane and ternary mixtures of n-butane, n-heptane and n-hexadecane, Fluid Phase Equilibria (2001), https://doi.org/10.1016/S0378-3812(01)00483-6.

[39] M. Medina-Bermúdez, L.A. Saavedra-Molina, W. Escamilla-Tiburcio, L.A. Galicia-Luna, O. Elizalde-Solis, P, ρ, T) behavior for the binary mixtures carbon dioxide + heptane and carbon dioxide + tridecane, J. Chem. Eng. Data 58 (2013) 1255–1264, https://doi.org/10.1021/je400056z.

[40] S.J. Ashcroft, M.B. Isa, Effect of dissolved gases on the densities of hydrocarbons, J. Chem. Eng. Data 42 (1997) 1244–1248, https://doi.org/10.1021/je9701588.

[41] Y. Zhang, Z. Liu, W. Liu, J. Zhao, M. Yang, Y. Liu, D. Wang, Y. Song, Measurement and modeling of the densities for CO_2 + dodecane system from 313.55 k to 353.55 k and pressures up to 18 MPa, J. Chem. Eng. Data 59 (2014) 3668–3676, https://doi.org/10.1021/je5005643.

[42] J. Zambrano, F.V. Gómez-Soto, D. Lozano-Martín, M.C. Martín, J.J. Segovia, Volumetric behaviour of (carbon dioxide + hydrocarbon) mixtures at high pressures, J. Supercrit. Fluids 110 (2016) 103–109, https://doi.org/10.1016/j.supflu.2016.01.002.

[43] D.C. Santos, I.S. Gonçalves, A. Mehl, P. Couto, M.L.L. Paredes, Density of *n*-Heptane + *n*-Dodecane and carbon dioxide + *n*-Heptane + *n*-Dodecane mixtures up to 70 MPa from (293.15 to 363.15) k, J. Chem. Eng. Data 66 (2021) 1305–1318, https://doi.org/10.1021/acs.jced.0c00943.

[44] C.A. Eckert, D.H. Ziger, K.P. Johnston, T.K. Ellison, The use of partial molal volume data to evaluate equations of state for supercritical fluid mixtures, Fluid Phase Equilibria 14 (1983) 167–175, https://doi.org/10.1016/0378-3812(83)80122-8.

[45] Z.S. Gonenc, U. Akman, A.K. Sunol, Solubility and partial molar volumes of naphthalene, phenanthrene, benzoic acid, and 2-Methoxynaphthalene in supercritical carbon dioxide, J. Chem. Eng. Data 40 (1995) 799–804, https://doi.org/10.1021/je00020a013.

[46] Y. Guo, A. Akgerman, Infinite dilution partial molar volumes of butanal and *2*-methylpropanal in supercritical carbon dioxide, J. Chem. Eng. Data 43 (1998) 889–892, https://doi.org/10.1021/je9800712.

[47] D.M. Pfund, L.L. Lee, H.D. Cochran, Application of the kirkwood-buff theory of solutions to dilute supercritical mixtures. Ii. the excluded volume and local composition models, Fluid Phase Equilibria 39 (1988) 161–192, https://doi.org/10.1016/0378-3812(88)85003-9.